

Correlated Dirac Eigenvalues and Axial Anomaly in Chiral Symmetric QCD

H.-T. Ding,¹ S.-T. Li,^{2,1} Swagato Mukherjee,³ A. Tomiya,⁴ X.-D. Wang,¹ and Y. Zhang^{1,*}

¹*Key Laboratory of Quark and Lepton Physics (MOE) and Institute of Particle Physics, Central China Normal University, Wuhan 430079, China*

²*Institute of Modern Physics, Chinese Academy of Sciences, Lanzhou 730000, China*

³*Physics Department, Brookhaven National Laboratory, Upton, New York 11973, USA*

⁴*RIKEN-BNL Research Center, Brookhaven National Laboratory, Upton, New York 11973, USA*

We introduce novel relations between the derivatives $[\partial^n \rho(\lambda, m_l)/\partial m_l^n]$ of the Dirac eigenvalue spectrum $[\rho(\lambda, m_l)]$ with respect to the light sea quark mass (m_l) and the $(n+1)$ -point correlations among the eigenvalues (λ) of the massless Dirac operator. Using these relations we present lattice QCD results for $\partial^n \rho(\lambda, m_l)/\partial m_l^n$ ($n = 1, 2, 3$) for m_l corresponding to pion masses $m_\pi = 160 - 55$ MeV, and at a temperature of about 1.6 times the chiral phase transition temperature. Calculations were carried out using (2+1) flavors of highly improved staggered quarks with the physical value of strange quark mass, three lattice spacings $a = 0.12, 0.08, 0.06$ fm, and lattices having aspect ratios 4–9. We find that $\rho(\lambda \rightarrow 0, m_l)$ develops a peaked structure. This peaked structure arises due to non-Poisson correlations within the infrared part of the Dirac eigenvalue spectrum, becomes sharper as $a \rightarrow 0$, and its amplitude is proportional to m_l^2 . We demonstrate that this $\rho(\lambda \rightarrow 0, m_l)$ is responsible for the manifestations of axial anomaly in two-point correlation functions of light scalar and pseudoscalar mesons. After continuum and chiral extrapolations we find that axial anomaly remains manifested in two-point correlation functions of scalar and pseudoscalar mesons in the chiral limit.

Introduction.— The Lagrangian of the (2+1)-flavor quantum chromodynamics (QCD) with the physical value of strange quark mass (m_s) and degenerate up and down light quarks possesses $SU(2)_L \times SU(2)_R$ chiral symmetry and $U(1)_A$ axial symmetry in the chiral limit of light quark mass $m_l \rightarrow 0$. The chiral symmetry is spontaneously broken in the vacuum and the $U(1)_A$ symmetry is anomalously broken due to quantum interactions. For the physical value of m_l , the broken chiral symmetry of the QCD vacuum gets approximately restored through a smooth crossover at a high temperature $T \simeq 156$ MeV [1–6], and for $m_l \rightarrow 0$ the restoration takes place via a chiral phase transition at a temperature $T_c = 132^{+3}_{-6}$ MeV [7].

Owing to the asymptotic freedom of QCD, the $U(1)_A$ axial symmetry becomes an exact symmetry only for $T \rightarrow \infty$. However, the nature of the chiral phase transition crucially depends on how axial anomaly manifests itself in the two-point correlation functions of light scalar and pseudoscalar mesons for $T \geq T_c$. If the isotriplet scalar δ and the isotriplet pseudoscalar π remain non-degenerate at $T \geq T_c$, then the chiral phase transition is expected to be of second order, belonging to a three-dimensional $O(4)$ universality class [8]. But if the δ and π become degenerate at $T \geq T_c$, then the chiral phase transition can be either first [8] or second order [9–11]. For the physical value of m_l , the δ and π remain non-degenerate around the chiral crossover [3, 12–15]. However, what happens for $T \simeq T_c$ as $m_l \rightarrow 0$ remains an open question [16–23] due to the lack of state-of-the-art lattice QCD calculations with controlled continuum and chiral extrapolations.

It has been shown that if Dirac eigenvalue spectrum $\rho(\lambda, m_l)$ is an analytic function of m_l^2 and λ then in the chiral limit $U(1)_A$ anomaly will not be manifested

in differences of up to six-point correlation functions of π and δ that can be connected via a $U(1)_A$ rotation [24]. However, weakly interacting instanton [25, 26] gas motivated $\rho \sim m_l^2 \delta(\lambda)$ can lead to nondegeneracy of the two-point π and δ correlation functions even as $m_l \rightarrow 0$ [13]. While the m_l^2 factor naturally arises from the two light fermion determinants, the $\delta(\lambda)$ -like structure is motivated by the limit when the small shift from zero to the near-zero modes, resulting from the weak interactions among localized (quasi) instantons and anti-instantons, can be neglected [27, 28]. Lattice QCD studies show that, for the physical values of m_l and for sufficiently high temperatures, the T dependence of a $U(1)_A$ -breaking measure, the topological susceptibility, follows dilute instanton gas approximation prediction (for a recent review, see [29]). However, whether these findings arise due to an underlying structure of $\rho \sim m_l^2 \delta(\lambda)$ and what happens for $m_l \rightarrow 0$ have remained unanswered. Some lattice QCD studies have observed infrared enhancement in ρ [13, 14, 19, 30, 31], however, whether such enhancements scale as m_l^2 as $m_l \rightarrow 0$ have not been demonstrated. In other lattice QCD calculations, no infrared enhancement in ρ was observed [17, 18, 20, 22], showing the importance of controlling lattice artifacts through continuum extrapolations. On the other hand, in Ref. [32] it was argued that if π and δ were to remain nondegenerate at $T \geq T_c$, then chiral symmetry restoration demands non-Poisson correlations among the infrared eigenvalues.

In this Letter we connect all the above issues: first, by establishing novel relations between $\partial^n \rho/\partial m_l^n$ and correlation among the eigenvalues, then by obtaining $\partial^n \rho/\partial m_l^n$ from state-of-the-art lattice QCD calculations. Finally, we demonstrate how the signature of axial

anomaly in two-point δ and π correlation functions arises as $m_l \rightarrow 0$.

$\partial^n \rho / \partial m_l^n$ and $U(1)_A$ anomaly. – For (2+1)-flavor QCD, the Dirac eigenvalue spectrum is given by

$$\rho(\lambda, m_l) = \frac{T}{VZ[\mathcal{U}]} \int \mathcal{D}[\mathcal{U}] e^{-S_G[\mathcal{U}]} \det [\not{D}[\mathcal{U}] + m_s] \times (\det [\not{D}[\mathcal{U}] + m_l])^2 \rho_U(\lambda). \quad (1)$$

Here, $\rho_U(\lambda) = \sum_j \delta(\lambda - \lambda_j)$, λ_j are the eigenvalues of the massless Dirac matrix $\not{D}[\mathcal{U}]$ for a given background SU(3) gauge field \mathcal{U} , V is the spatial volume, $S_G[\mathcal{U}]$ is the gauge action, and the partition function $Z[\mathcal{U}] = \int \mathcal{D}[\mathcal{U}] e^{-S_G[\mathcal{U}]} \det [\not{D}[\mathcal{U}] + m_s] (\det [\not{D}[\mathcal{U}] + m_l])^2$. Note that $\rho_U(\lambda)$ does not explicitly depend on m_l , however, m_l dependence enters ρ through the integration over the gauge fields. Furthermore,

$$\begin{aligned} \det [\not{D}[\mathcal{U}] + m_l] &= \prod_j (+i\lambda_j + m_l)(-i\lambda_j + m_l) \\ &= \exp \left(\int_0^\infty d\lambda \rho_U(\lambda) \ln [\lambda^2 + m_l^2] \right). \end{aligned} \quad (2)$$

Substituting Eq. 2 in Eq. 1 and $Z[\mathcal{U}]$ it is straightforward to obtain $\partial^n \rho / \partial m_l^n$, e.g.,

$$\begin{aligned} \frac{V}{T} \frac{\partial \rho}{\partial m_l} &= \int_0^\infty d\lambda_2 \frac{4m_l C_2(\lambda, \lambda_2; m_l)}{\lambda_2^2 + m_l^2}, \\ \frac{V}{T} \frac{\partial^2 \rho}{\partial m_l^2} &= \int_0^\infty d\lambda_2 \frac{4(\lambda_2^2 - m_l^2) C_2(\lambda, \lambda_2; m_l)}{(\lambda_2^2 + m_l^2)^2} \\ &\quad + \int_0^\infty d\lambda_2 d\lambda_3 \frac{(4m_l)^2 C_3(\lambda, \lambda_2, \lambda_3; m_l)}{(\lambda_2^2 + m_l^2)(\lambda_3^2 + m_l^2)}, \quad \text{with} \end{aligned} \quad (3)$$

$$C_n(\lambda_1, \dots, \lambda_n; m_l) = \left\langle \prod_{i=1}^n [\rho_U(\lambda_i) - \langle \rho_U(\lambda_i) \rangle] \right\rangle. \quad (5)$$

The difference of the integrated two-point functions, i.e., susceptibilities, of the isotriplet pseudoscalar, $\pi^i(x) = i\bar{\psi}_l(x)\gamma_5\tau^i\psi_l(x)$, and the isotriplet scalar, $\delta^i(x) = \bar{\psi}_l(x)\tau^i\psi_l(x)$, mesons is defined as

$$\chi_\pi - \chi_\delta = \int d^4x \langle \pi^i(x)\pi^i(0) - \delta^i(x)\delta^i(0) \rangle. \quad (6)$$

For $T \geq T_c$ owing to the degeneracy of π and the isosinglet scalar meson in the chiral limit [13]

$$\chi_\pi - \chi_\delta = \chi_{\text{disc}}, \quad (7)$$

where χ_{disc} is the quark-line disconnected part of the isosinglet scalar meson susceptibility [33],

$$\chi_{\text{disc}} = \frac{T}{V} \int d^4x \langle [\bar{\psi}(x)\psi(x) - \langle \bar{\psi}(x)\psi(x) \rangle]^2 \rangle. \quad (8)$$

These $U(1)_A$ symmetry-breaking measures are related to ρ through [13, 32, 34]

$$\chi_\pi - \chi_\delta = \int_0^\infty d\lambda \frac{8m_l^2 \rho}{(\lambda^2 + m_l^2)^2}, \quad (9)$$

$$\chi_{\text{disc}} = \int_0^\infty d\lambda \frac{4m_l \partial \rho / \partial m_l}{\lambda^2 + m_l^2}. \quad (10)$$

In the Poisson limit, C_n is given by: $C_n^{\text{Po}}(\lambda_1, \dots, \lambda_n) = \delta(\lambda_1 - \lambda_2) \cdots \delta(\lambda_n - \lambda_{n-1}) \langle (\rho_U(\lambda_1) - \langle \rho_U(\lambda_1) \rangle)^n \rangle = \delta(\lambda_1 - \lambda_2) \cdots \delta(\lambda_n - \lambda_{n-1}) \langle \rho_U(\lambda_1) \rangle + \mathcal{O}(1/N)$, where $2N \propto V/T$ is the total number of eigenvalues. In this limit,

$$\left(\frac{\partial \rho}{\partial m_l} \right)^{\text{Po}} = \frac{4m_l \rho}{\lambda^2 + m_l^2} - \frac{V \rho}{TN} \langle \bar{\psi} \psi \rangle, \quad (11)$$

$$\begin{aligned} \left(\frac{\partial^2 \rho}{\partial m_l^2} \right)^{\text{Po}} &= \frac{4\rho}{\lambda^2 + m_l^2} + \frac{8m_l^2 \rho}{(\lambda^2 + m_l^2)^2} + \frac{2V^2 \rho}{T^2 N^2} \langle \bar{\psi} \psi \rangle^2 \\ &\quad - \frac{V \rho}{TN} \left(\frac{8m_l \langle \bar{\psi} \psi \rangle}{\lambda^2 + m_l^2} + 2\chi_\pi - \chi_\delta \right), \end{aligned} \quad (12)$$

where $\langle \bar{\psi} \psi \rangle = (T/V)(d \ln Z[\mathcal{U}] / dm_l)$. In the chiral limit, this leads to $\chi_{\text{disc}}^{\text{Po}} = 2(\chi_\pi - \chi_\delta)$, in clear violation of the chiral symmetry restoration condition in Eq. 7, unless both sides of the equation trivially vanish.

Lattice QCD calculations. – Lattice QCD calculations were carried out at $T \approx 205 \text{ MeV} \approx 1.6T_c$ for (2+1)-flavor QCD using the highly improved staggered quarks and the tree-level Symanzik gauge action, a setup extensively used by the HotQCD Collaboration [2, 5, 35–37]. The m_s was tuned to its physical value and three lattice spacings $a = (TN_\tau)^{-1} = 0.12, 0.08, 0.06 \text{ fm}$, corresponding to lattice temporal extents $N_\tau = 8, 12, 16$, were used [15]. Calculations were done with $m_l = m_s/20, m_s/27, m_s/40, m_s/80, m_s/160$ that correspond to $m_\pi \simeq 160, 140, 110, 80, 55 \text{ MeV}$, respectively. The spatial extents (N_σ) of the lattices were chosen to have aspect ratios in the range of $N_\sigma/N_\tau = 4 - 9$. The gauge field configurations were generated using the rational hybrid Monte Carlo algorithm [38, 39]. Gauge configurations from every 10th molecular dynamics trajectory of unit length were saved to carry out various measurements. ρ and C_n were computed by measuring $\rho_U(\lambda)$ over the entire range of λ using the Chebyshev filtering technique combined with the stochastic estimate method [40–44] on ~ 2000 configurations. Orders of the Chebyshev polynomials were chosen to be $(1 - 5) \times 10^5$ and 24 Gaussian stochastic sources were used. Measurements of χ_{disc} and $\chi_\pi - \chi_\delta$ were done by inverting the light fermion matrix using 50 Gaussian random sources on 2000 – 10000 configurations [45].

Results. – Fig. 1 (left) shows the m_l dependence of $m_l^{-1} \partial \rho / \partial m_l$ and $\partial^2 \rho / \partial m_l^2$ at $T \approx 1.6T_c$, obtained for lattices with $N_\tau = 8$ and the largest available

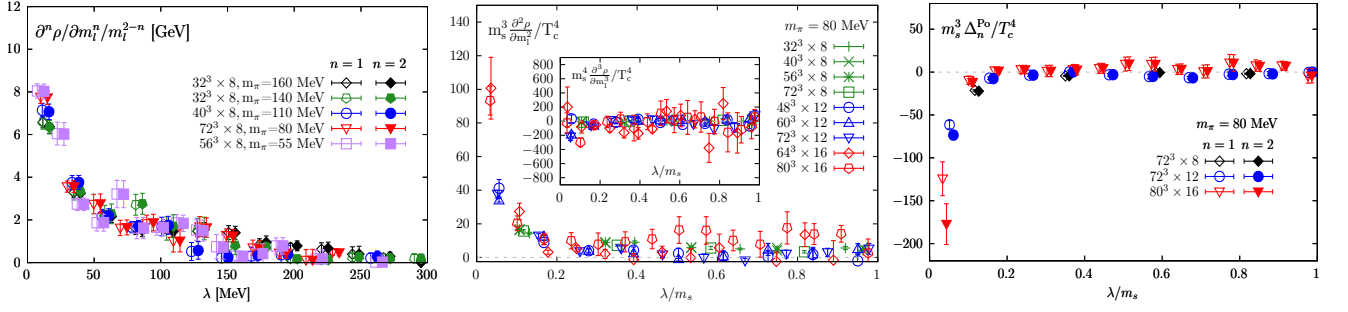


FIG. 1. Left: Light sea quark mass dependence of $m_l^{-1} \partial \rho(\lambda, m_l) / \partial m_l$ (open symbols) and $\partial^2 \rho(\lambda, m_l) / \partial m_l^2$ (filled symbols) using $N_\tau = 8$ lattices. Middle: Lattice spacing and volume dependence of $\partial^2 \rho(\lambda, m_l) / \partial m_l^2$ and $\partial^3 \rho(\lambda, m_l) / \partial m_l^3$ (inset) for $m_\pi = 80$ MeV. Right: The differences, $\Delta_n^{\text{Po}} = m_l^{n-2} [\partial^n \rho / \partial m_l^n - (\partial^n \rho / \partial m_l^n)^{\text{Po}}]$ [cf. Eq. 11 and Eq. 12], for $m_\pi = 80$ MeV and three lattice spacings. In all cases, results are obtained at $T \approx 205$ MeV and the filled symbols have been slightly shifted horizontally for visibility.

N_σ for that m_l . We observe that $m_l^{-1} (\partial \rho / \partial m_l)$ and $\partial^2 \rho / \partial m_l^2$ are almost identical and independent of m_l . Also, $m_l^{-1} \partial \rho / \partial m_l$ and $\partial^2 \rho / \partial m_l^2$ are peaked at $\lambda \rightarrow 0$ and drop rapidly toward zero for $\lambda/T \gtrsim 1$. Fig. 1 (middle) depicts the lattice spacing and volume dependence of $\partial^2 \rho / \partial m_l^2$ and $\partial^3 \rho / \partial m_l^3$ for $m_\pi = 80$ MeV. To compare these quantities across different lattice spacings we multiply with the appropriate powers of m_s to make them renormalization group invariant and make them dimensionless by rescaling with appropriate powers of $T_c = 132$ MeV. We see that the peaked structure in $\partial^2 \rho / \partial m_l^2$ at $\lambda \rightarrow 0$ becomes sharper as $a \rightarrow 0$, and shows little volume dependence (see Supplemental Material [46]). Moreover, within errors, $\partial^3 \rho / \partial m_l^3$ are found to be consistent with zero in all the cases. The findings $m_l^{-1} \partial \rho / \partial m_l \approx \partial^2 \rho / \partial m_l^2$ and $\partial^3 \rho / \partial m_l^3 \approx 0$ show that the peaked structure $\rho(\lambda \rightarrow 0, m_l \rightarrow 0) \propto m_l^2$. In Fig. 1 (right) we show the difference $\Delta_n^{\text{Po}} = m_l^{n-2} [\partial^n \rho / \partial m_l^n - (\partial^n \rho / \partial m_l^n)^{\text{Po}}]$ ($n = 1, 2$), with the Poisson approximations for $\partial^n \rho / \partial m_l^n$ as defined in Eq. 11 and Eq. 12. The fact $\Delta_n^{\text{Po}} < 0$ shows that the repulsive non-Poisson correlation within the small λ gives rise to the $\rho(\lambda \rightarrow 0)$ peak.

In Fig. 2 we show that ρ and $\partial \rho / \partial m_l$ reproduce directly measured $\chi_\pi - \chi_\delta$ and χ_{disc} using Eq. 9 and Eq. 10, respectively. The numerical integrations in λ were performed using the rectangle method, where the largest value of λ was estimated using the power method and the statistical error of integration was obtained using the jackknife method. Since we saw very mild volume dependence in all the quantities, we only present results from the largest available volume for each N_τ and m_l . We checked that only the infrared $\lambda/T \lesssim 1$ parts of ρ and $\partial \rho / \partial m_l$ are needed for the reproductions of $\chi_\pi - \chi_\delta$ and χ_{disc} , within errors, for all N_τ and m_l . Additionally, we checked that once the bin-size of λ in the numerical integration of Eq. 9 is chosen to reproduce directly measured $\chi_\pi - \chi_\delta$, the same bin size automatically reproduces χ_{disc} and $\langle \bar{\psi} \psi \rangle$ without any further tuning. We observe that

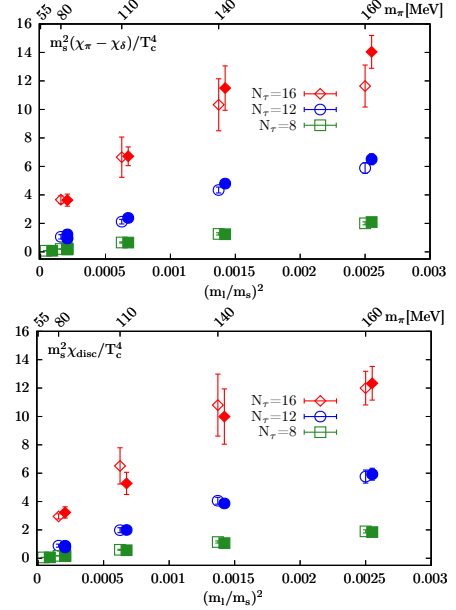


FIG. 2. Comparisons of direct measurements (open symbols) of $\chi_\pi - \chi_\delta$ (top) and χ_{disc} (bottom) with those reconstructed (filled symbols, slightly shifted horizontally for visibility) from ρ [cf. Eq. 9] and $\partial \rho / \partial m_l$ [cf. Eq. 10], respectively. The results are shown for all values of light quark masses and lattice spacings at $T \approx 205$ MeV.

both χ_{disc} and $\chi_\pi - \chi_\delta$ are linear in m_l^2 for all lattice spacings and especially for $m_\pi \lesssim 140$ MeV; this is in accord with the expectation $Z[\mathcal{U}]$ is an even function of m_l for $T \geq T_c$ due to the restoration of the $Z(2)$ subgroup of $SU(2)_L \times SU(2)_R$.

In Fig. 3 we show the continuum and chiral extrapolated results for χ_{disc} and $\chi_\pi - \chi_\delta$. Using all the data for $N_\tau = 8, 12, 16$ and $m_\pi \leq 140$ MeV, we performed a joint $a, m_l \rightarrow 0$ extrapolation of the form $\chi_{\text{disc}}(a, m_l) = \chi_{\text{disc}}(0, 0) + a_1/N_\tau^2 + a_2/N_\tau^4 + (m_l/m_s)^2 [b_0 + b_1/N_\tau^2 + b_2/N_\tau^4]$. Fits were performed on

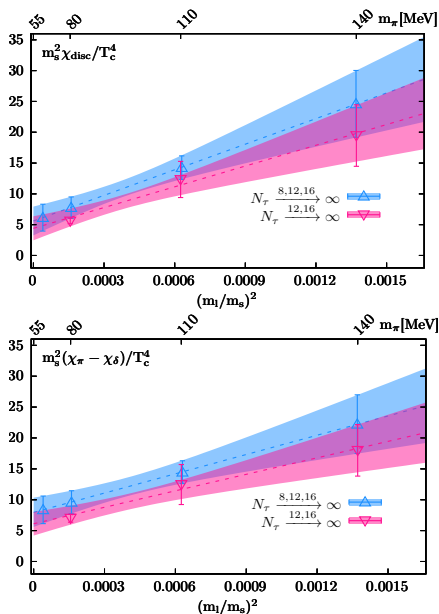


FIG. 3. Continuum and chiral extrapolated results for χ_{disc} (top) and $\chi_{\pi} - \chi_{\delta}$ (bottom) at $T \approx 205$ MeV. See text for details.

each bootstrap sample of the data set. The bootstrap samples were created by randomly choosing data from Gaussian distributions with means equal to the average values and variances equal to the $1\text{-}\sigma$ errors of the directly measured χ_{disc} . We chose the median value of the resulting bootstrap distribution as the final result (depicted by the upward triangles) and the 68% percentiles confidence interval of the resulting distribution as the errors on the final results (the band labeled by $N_{\tau} \xrightarrow{8,12,16} \infty$). Since we used the so-called rooted-staggered formulation [47–50] for our (2+1)-flavor lattice QCD, we also checked that the same $\chi_{\text{disc}}(0,0)$ is obtained within errors by first carrying out the $a \rightarrow 0$ extrapolations for each m_l and then performing the $m_l \rightarrow 0$ extrapolation using the $a \rightarrow 0$ extrapolated results. For this purpose, we used the $N_{\tau} = 12, 16$ data for each of $m_l = m_s/27, m_s/40, m_s/80$ to obtain $\chi_{\text{disc}}(0, m_l)$ by fitting to the ansatz $\chi_{\text{disc}}(a, m_l) = \chi_{\text{disc}}(0, m_l) + d_1/N_{\tau}^2$. Then the chiral extrapolation was carried out using $\chi_{\text{disc}}(0, m_l) = \chi_{\text{disc}}(0, 0) + d_2(m_l/m_s)^2$ based on the continuum estimates of $\chi_{\text{disc}}(0, m_l)$. These extrapolations were done by using the same bootstrap procedure described before and the final results are indicated with the label $N_{\tau} \xrightarrow{12,16} \infty$. Exactly the same procedures were followed also for $\chi_{\pi} - \chi_{\delta}$ to obtain its continuum and chiral extrapolated values. After carrying out continuum and chiral extrapolations we find that Eq. 7 is satisfied within errors, and χ_{disc} and $\chi_{\pi} - \chi_{\delta}$ are nonvanishing at a confidence level above 95%.

Conclusions.— In this Letter we establish relations between $\partial^n \rho / \partial m_l^n$ and C_{n+1} . To the best of our knowl-

edge these relations are new in the literature. Based on these relations, for the first time, we present direct computations of $\partial^n \rho / \partial m_l^n$ employing state-of-the-art lattice QCD techniques. The results presented in this Letter led us to conclude that, in chiral symmetric (2+1)-flavor QCD at $T \approx 1.6T_c$, (i) $\rho(\lambda \rightarrow 0, m_l)$ develops a peaked structure due to repulsive non-Poisson correlations within small λ ; the peak becomes sharper as $a \rightarrow 0$, and its amplitude is $\propto m_l^2$. (ii) The underlying presence of this $\rho(\lambda \rightarrow 0, m_l)$ leads to manifestations of $U(1)_A$ anomaly in $\chi_{\pi} - \chi_{\delta}$ and χ_{disc} . (iii) Axial anomaly remains manifested in $\chi_{\pi} - \chi_{\delta}$ and χ_{disc} even in the chiral limit. These suggest that for $T \gtrsim 1.6T_c$ the microscopic origin of axial anomaly is driven by the weakly interacting (quasi)instanton gas motivated $\rho(\lambda \rightarrow 0, m_l \rightarrow 0) \sim m_l^2 \delta(\lambda)$, and the chiral phase transition in (2+1)-flavor QCD is of the three-dimensional $O(4)$ universality class.

The above conclusions are based on the continuum extrapolated lattice QCD calculations using the (2+1) flavors of staggered fermions. Confirmations of these continuum extrapolated results using other fermion actions, especially using chiral fermions, are needed in future. Even in those future calculations it will be very difficult to directly identify a structure like $m_l^2 \delta(\lambda)$ in ρ itself as $m_l \rightarrow 0$. The formalism developed and techniques presented in this Letter for directly accessing $\partial^n \rho / \partial m_l^n$ will be essential for those future studies too. The same or similar formalism also may have many potential applications beyond the present physics problem: few plausible examples testing the predictions of random matrix theory [34, 51, 52], determination of strong coupling constant using Dirac eigenvalue spectrum [53], determinations of mass anomalous dimensions in different theories [54–58], etc.

This material is based upon work supported by the National Natural Science Foundation of China under Grants No. 11775096, No. 11535012, and No. 11947237; the U.S. Department of Energy, Office of Science, Office of Nuclear Physics through the Award No. DE-SC0012704; the U.S. Department of Energy, Office of Science, Office of Nuclear Physics and Office of Advanced Scientific Computing Research within the framework of Scientific Discovery through Advance Computing (SciDAC) award Computing the Properties of Matter with Leadership Computing Resources; and RIKEN Special Postdoctoral Researcher program and JSPS KAKENHI Grant No. JP20K14479. Computations for this work were carried out on the GPU clusters of the Nuclear Science Computing Center at Central China Normal University (NSC³), Wuhan, China, and facilities of the USQCD Collaboration, which are funded by the Office of Science of the U.S. Department of Energy. For generating the gauge configurations, the HotQCD software suite was used, and the eigenvalue measurement code was developed also based on the same software suite. We are in-

debted to the HotQCD Collaboration for sharing their software suite with us.

-
- * yuzhang@mails.cnu.edu.cn
- [1] Y. Aoki, S. Borsanyi, S. Durr, Z. Fodor, S. D. Katz, S. Krieg, and K. K. Szabo, *JHEP* **06**, 088 (2009), [arXiv:0903.4155](https://arxiv.org/abs/0903.4155) [hep-lat].
- [2] A. Bazavov, T. Bhattacharya, M. Cheng, C. DeTar, H. Ding, *et al.*, *Phys.Rev.* **D85**, 054503 (2012), [arXiv:1111.1710](https://arxiv.org/abs/1111.1710) [hep-lat].
- [3] T. Bhattacharya, M. I. Buchoff, N. H. Christ, H.-T. Ding, R. Gupta, *et al.*, *Phys.Rev.Lett.* **113**, 082001 (2014), [arXiv:1402.5175](https://arxiv.org/abs/1402.5175) [hep-lat].
- [4] C. Bonati, M. D'Elia, M. Mariti, M. Mesiti, F. Negro, and F. Sanfilippo, *Phys. Rev.* **D92**, 054503 (2015), [arXiv:1507.03571](https://arxiv.org/abs/1507.03571) [hep-lat].
- [5] A. Bazavov *et al.* (HotQCD), *Phys. Lett.* **B795**, 15 (2019), [arXiv:1812.08235](https://arxiv.org/abs/1812.08235) [hep-lat].
- [6] S. Borsanyi, Z. Fodor, J. N. Guenther, R. Kara, S. D. Katz, P. Parotto, A. Pasztor, C. Ratti, and K. K. Szabo, *Phys. Rev. Lett.* **125**, 052001 (2020), [arXiv:2002.02821](https://arxiv.org/abs/2002.02821) [hep-lat].
- [7] H. T. Ding *et al.*, *Phys. Rev. Lett.* **123**, 062002 (2019), [arXiv:1903.04801](https://arxiv.org/abs/1903.04801) [hep-lat].
- [8] R. D. Pisarski and F. Wilczek, *Phys.Rev.* **D29**, 338 (1984).
- [9] A. Butti, A. Pelissetto, and E. Vicari, *JHEP* **08**, 029 (2003), [arXiv:hep-ph/0307036](https://arxiv.org/abs/hep-ph/0307036) [hep-ph].
- [10] A. Pelissetto and E. Vicari, *Phys. Rev.* **D88**, 105018 (2013), [arXiv:1309.5446](https://arxiv.org/abs/1309.5446) [hep-lat].
- [11] M. Grahl, *Phys. Rev.* **D90**, 117904 (2014), [arXiv:1410.0985](https://arxiv.org/abs/1410.0985) [hep-th].
- [12] M. Cheng *et al.*, *Eur. Phys. J. C* **71**, 1564 (2011), [arXiv:1010.1216](https://arxiv.org/abs/1010.1216) [hep-lat].
- [13] A. Bazavov *et al.* (HotQCD), *Phys.Rev.* **D86**, 094503 (2012), [arXiv:1205.3535](https://arxiv.org/abs/1205.3535) [hep-lat].
- [14] M. I. Buchoff, M. Cheng, N. H. Christ, H. T. Ding, C. Jung, *et al.*, *Phys.Rev.* **D89**, 054514 (2014), [arXiv:1309.4149](https://arxiv.org/abs/1309.4149) [hep-lat].
- [15] A. Bazavov *et al.*, *Phys. Rev. D* **100**, 094510 (2019), [arXiv:1908.09552](https://arxiv.org/abs/1908.09552) [hep-lat].
- [16] H. Ohno, U. Heller, F. Karsch, and S. Mukherjee, *PoS LATTICE2012*, 095 (2012), [arXiv:1211.2591](https://arxiv.org/abs/1211.2591) [hep-lat].
- [17] G. Cossu, S. Aoki, H. Fukaya, S. Hashimoto, T. Kaneko, *et al.*, *Phys.Rev.* **D87**, 114514 (2013), [arXiv:1304.6145](https://arxiv.org/abs/1304.6145) [hep-lat].
- [18] T.-W. Chiu, W.-P. Chen, Y.-C. Chen, H.-Y. Chou, and T.-H. Hsieh (TWQCD), *PoS LATTICE2013*, 165 (2014), [arXiv:1311.6220](https://arxiv.org/abs/1311.6220) [hep-lat].
- [19] V. Dick, F. Karsch, E. Laermann, S. Mukherjee, and S. Sharma, *Phys. Rev.* **D91**, 094504 (2015), [arXiv:1502.06190](https://arxiv.org/abs/1502.06190) [hep-lat].
- [20] A. Tomiya, G. Cossu, S. Aoki, H. Fukaya, S. Hashimoto, T. Kaneko, and J. Noaki, *Phys. Rev. D* **96**, 034509 (2017), [Addendum: *Phys.Rev.D* 96, 079902 (2017)], [arXiv:1612.01908](https://arxiv.org/abs/1612.01908) [hep-lat].
- [21] B. B. Brandt, A. Francis, H. B. Meyer, O. Philipsen, D. Robaina, and H. Wittig, (2016), [arXiv:1608.06882](https://arxiv.org/abs/1608.06882) [hep-lat].
- [22] K. Suzuki, S. Aoki, Y. Aoki, G. Cossu, H. Fukaya, S. Hashimoto, and C. Rohrhofer (JLQCD), in *37th International Symposium on Lattice Field Theory (Lattice 2019) Wuhan, Hubei, China, June 16-22, 2019* (2020) [arXiv:2001.07962](https://arxiv.org/abs/2001.07962) [hep-lat].
- [23] S. Aoki, Y. Aoki, G. Cossu, H. Fukaya, S. Hashimoto, T. Kaneko, C. Rohrhofer, and K. Suzuki (JLQCD), (2020), [arXiv:2011.01499](https://arxiv.org/abs/2011.01499) [hep-lat].
- [24] S. Aoki, H. Fukaya, and Y. Taniguchi, *Phys.Rev.* **D86**, 114512 (2012), [arXiv:1209.2061](https://arxiv.org/abs/1209.2061) [hep-lat].
- [25] G. 't Hooft, *Phys. Rev. Lett.* **37**, 8 (1976).
- [26] G. 't Hooft, *Phys. Rev. D* **14**, 3432 (1976), [Erratum: *Phys.Rev.D* 18, 2199 (1978)].
- [27] D. J. Gross, R. D. Pisarski, and L. G. Yaffe, *Rev. Mod. Phys.* **53**, 43 (1981).
- [28] T. Kanazawa and N. Yamamoto, *Phys. Rev.* **D91**, 105015 (2015), [arXiv:1410.3614](https://arxiv.org/abs/1410.3614) [hep-th].
- [29] M. P. Lombardo and A. Trunin, *Int. J. Mod. Phys. A* **35**, 2030010 (2020), [arXiv:2005.06547](https://arxiv.org/abs/2005.06547) [hep-lat].
- [30] A. Alexandru and I. Horváth, *Phys. Rev. D* **92**, 045038 (2015), [arXiv:1502.07732](https://arxiv.org/abs/1502.07732) [hep-lat].
- [31] A. Alexandru and I. Horváth, *Phys. Rev. D* **100**, 094507 (2019), [arXiv:1906.08047](https://arxiv.org/abs/1906.08047) [hep-lat].
- [32] T. Kanazawa and N. Yamamoto, *JHEP* **01**, 141 (2016), [arXiv:1508.02416](https://arxiv.org/abs/1508.02416) [hep-th].
- [33] The term $\langle \bar{\psi}\psi \rangle^2$ arises naturally from $\partial \langle \bar{\psi}\psi \rangle / \partial m_l$, and trivially vanishes for $T \geq T_c$ as $m_l \rightarrow 0$. Following standard convention, this term was subtracted off to cancel the $(m_l/a)^2$ divergence.
- [34] D. Toublan and J. J. M. Verbaarschot, *Nucl. Phys.* **B603**, 343 (2001), [arXiv:hep-th/0012144](https://arxiv.org/abs/hep-th/0012144) [hep-th].
- [35] A. Bazavov *et al.* (HotQCD Collaboration), *Phys.Rev.* **D90**, 094503 (2014), [arXiv:1407.6387](https://arxiv.org/abs/1407.6387) [hep-lat].
- [36] A. Bazavov *et al.* (HotQCD Collaboration), *Phys.Rev.* **D86**, 034509 (2012), [arXiv:1203.0784](https://arxiv.org/abs/1203.0784) [hep-lat].
- [37] A. Bazavov *et al.*, *Phys. Rev.* **D95**, 054504 (2017), [arXiv:1701.04325](https://arxiv.org/abs/1701.04325) [hep-lat].
- [38] M. A. Clark, A. D. Kennedy, and Z. Sroczynski, *Lattice field theory. Proceedings, 22nd International Symposium, Lattice 2004, Batavia, USA, June 21-26, 2004*, *Nucl. Phys. Proc. Suppl.* **140**, 835 (2005), [arXiv:hep-lat/0409133](https://arxiv.org/abs/hep-lat/0409133) [hep-lat].
- [39] A. Bazavov *et al.* (MILC), *Phys. Rev.* **D82**, 074501 (2010), [arXiv:1004.0342](https://arxiv.org/abs/1004.0342) [hep-lat].
- [40] H.-T. Ding, O. Kaczmarek, F. Karsch, S.-T. Li, S. Mukherjee, A. Tomiya, and Y. Zhang, in *Proceedings, 37th International Symposium on Lattice Field Theory (Lattice 2019): Wuhan, China, June 16-22 2019* (2019) [arXiv:2001.05217](https://arxiv.org/abs/2001.05217) [hep-lat].
- [41] L. Giusti and M. Luscher, *JHEP* **03**, 013 (2009), [arXiv:0812.3638](https://arxiv.org/abs/0812.3638) [hep-lat].
- [42] G. Cossu, H. Fukaya, S. Hashimoto, T. Kaneko, and J.-I. Noaki, *PTEP* **2016**, 093B06 (2016), [arXiv:1607.01099](https://arxiv.org/abs/1607.01099) [hep-lat].
- [43] Z. Fodor, K. Holland, J. Kuti, S. Mondal, D. Nogradi, and C. H. Wong, *Proceedings, 33rd International Symposium on Lattice Field Theory (Lattice 2015): Kobe, Japan, July 14-18, 2015*, *PoS LATTICE2015*, 310 (2016), [arXiv:1605.08091](https://arxiv.org/abs/1605.08091) [hep-lat].
- [44] H.-T. Ding, S.-T. Li, A. Tomiya, X.-D. Wang, and Y. Zhang, (2020), [arXiv:2008.00493](https://arxiv.org/abs/2008.00493) [hep-lat].
- [45] χ_π was obtained through the Ward identity $m_l \chi_\pi = \langle \bar{\psi}\psi \rangle$ [44, 50] and χ_δ is the connected chiral susceptibility [14]. We checked that these results were reproduced, within errors, by the susceptibilities of the independently

computed π and δ 2-point correlation functions.

- [46] See Supplemental Material for the technical details of this study, which includes Refs. [2, 5, 32, 35–37, 40–44, 55, 59–63]. We also found that even when the same bin size in λ/m_s is used for all three lattice spacings the infrared peak structure persists as continuum limit is approached, see Fig. 11 of the Supplemental Material.
- [47] C. Bernard, *Phys. Rev. D* **71**, 094020 (2005), arXiv:hep-lat/0412030.
- [48] C. Bernard, M. Golterman, Y. Shamir, and S. R. Sharpe, *Phys. Lett. B* **649**, 235 (2007), arXiv:hep-lat/0603027.
- [49] S. R. Sharpe, *PoS LAT2006*, 022 (2006), arXiv:hep-lat/0610094.
- [50] G. W. Kilcup and S. R. Sharpe, *Nucl. Phys.* **B283**, 493 (1987).
- [51] J. Osborn and J. Verbaarschot, *Nucl. Phys. B* **525**, 738 (1998), arXiv:hep-ph/9803419.
- [52] A. S. Christensen, K. Splittorff, and J. Verbaarschot, *JHEP* **11**, 113 (2014), arXiv:1408.1498 [hep-lat].
- [53] K. Nakayama, H. Fukaya, and S. Hashimoto, *Phys. Rev. D* **98**, 014501 (2018), arXiv:1804.06695 [hep-lat].
- [54] A. Patella, *Phys. Rev. D* **84**, 125033 (2011), arXiv:1106.3494 [hep-th].
- [55] A. Patella, *Phys. Rev. D* **86**, 025006 (2012), arXiv:1204.4432 [hep-lat].
- [56] K. Cichy, *JHEP* **08**, 127 (2014), arXiv:1311.3572 [hep-lat].
- [57] A. Cheng, A. Hasenfratz, G. Petropoulos, and D. Schaich, *JHEP* **07**, 061 (2013), arXiv:1301.1355 [hep-lat].
- [58] N. Karthik and R. Narayanan, (2020), arXiv:2009.01313 [hep-lat].
- [59] A. Ramos and S. Sint, *Eur. Phys. J.* **C76**, 15 (2016), arXiv:1508.05552 [hep-lat].
- [60] E. Itou and A. Tomiya, *PoS LATTICE2014*, 252 (2014), arXiv:1411.1155 [hep-lat].
- [61] P. de Forcrand and B. Jager, *Proceedings, 35th International Symposium on Lattice Field Theory (Lattice 2017): Granada, Spain, June 18-24, 2017*, *EPJ Web Conf.* **175**, 14022 (2018), arXiv:1710.07305 [hep-lat].
- [62] E. D. Napoli, E. Polizzi, and Y. Saad, *CoRR abs/1308.4275* (2013), arXiv:1308.4275.
- [63] Y. Saad, *Numerical Methods for Large Eigenvalue Problems* (Society for Industrial and Applied Mathematics, 2011).

SUPPLEMENTAL MATERIALS

We provide supplemental materials in the sequence according to the contents in the main material.

I. $\partial^n \rho / m_l^n$ AND $U(1)_A$ ANOMALY

IA. Quantities related to ρ and $\partial^2 \rho / \partial m_l^2$

The two-flavor light quark chiral condensate $\langle \bar{\psi} \psi \rangle$ is related to the Dirac eigenvalue spectrum ρ as follows

$$\langle \bar{\psi} \psi \rangle = \int_0^\infty \frac{4m_l \rho}{\lambda^2 + m_l^2} d\lambda, \quad (13)$$

and it can also be expressed in terms of fermion matrix inverse M^{-1}

$$\langle \bar{\psi} \psi \rangle = \frac{T}{V} \frac{d \ln Z}{d m_l} = \frac{2T}{V} \text{Tr}(\not{D} + m_l)^{-1} \equiv \frac{2T}{V} \text{Tr} M^{-1}, \quad (14)$$

where M is the single-flavor fermion matrix. In our lattice QCD simulations staggered fermions are adopted and we thus deal with a 4-flavor fermion matrix M_{stag} . By utilizing the commonly used fourth-root technique [2, 5, 35–37] we have $\text{Tr} M^{-1} \equiv \frac{1}{4} \text{Tr} M_{stag}^{-1}$. The same applies to ρ , i.e. $\rho \equiv \rho_{stag}/4$ through our paper.

We define a quantity χ_2 which can be related to the second order derivative of ρ with respect to m_l as follows

$$\chi_2 = \int_0^\infty d\lambda \frac{4m_l \partial^2 \rho / \partial m_l^2}{\lambda^2 + m_l^2}. \quad (15)$$

The above quantity can also be evaluated in terms of M^{-1} ,

$$\begin{aligned} \chi_2 = \frac{4T}{V} & \left(2 \left(\langle (\text{Tr} M^{-1})^3 \rangle + 2 \langle \text{Tr} M^{-1} \rangle^3 - 3 \langle \text{Tr} M^{-1} \rangle \langle (\text{Tr} M^{-1})^2 \rangle \right) \right. \\ & \left. + \langle \text{Tr} M^{-1} \rangle \langle \text{Tr} M^{-2} \rangle - \langle \text{Tr} M^{-2} \text{Tr} M^{-1} \rangle \right). \end{aligned} \quad (16)$$

IB. Expressions for $\partial^n \rho / \partial m_l^n$ and C_{n+1} with $n=1,2,3$

One can work out the expressions for higher order correlation functions and m_l derivatives of ρ according to procedures described in the main material (*cf.* Eq. 1, Eq. 2, Eq. 3, Eq. 4 and Eq. 5) Here for demonstration we show expressions for up to third derivatives of ρ with respect to m_l , and up to four point correlation functions C_4 as well as χ_{disc} and χ_2 in the Poisson limits.

The third derivative of $\rho(\lambda, m_l)$ with respect to the light quark mass can be expressed as follows

$$\begin{aligned} \frac{V}{T} \frac{\partial^3 \rho(\lambda, m_l)}{\partial m_l^3} &= \int_0^\infty d\lambda_3 \int_0^\infty d\lambda_2 \int_0^\infty d\lambda_1 \frac{(4m_l)^3 C_4(\lambda, \lambda_1, \lambda_2, \lambda_3; m_l)}{(\lambda_3^2 + m_l^2)(\lambda_2^2 + m_l^2)(\lambda_1^2 + m_l^2)} \\ &+ \int_0^\infty d\lambda_2 \int_0^\infty d\lambda_1 \frac{48m_l(\lambda_2^2 - m_l^2) C_3(\lambda, \lambda_1, \lambda_2; m_l)}{(\lambda_2^2 + m_l^2)^2 (\lambda_1^2 + m_l^2)} \\ &+ \int_0^\infty d\lambda_1 \frac{8m_l(m_l^2 - 3\lambda_1^2) C_2(\lambda, \lambda_1; m_l)}{(\lambda_1^2 + m_l^2)^3}. \end{aligned} \quad (17)$$

where C_2 and C_3 are two-point and three-point correlation functions, respectively, as mentioned in the main text, and C_4 is the four point correlation function.

In the case that number of eigenvalues among gauge ensembles is Poisson distributed, the correlation functions are

reduced to

$$C_2^{\text{Po}}(\lambda_1, \lambda_2; m_l) = \frac{V}{T} \left(\delta(\lambda_1 - \lambda_2) \rho(\lambda_1, m_l) - \frac{V}{TN} \rho(\lambda_1, m_l) \rho(\lambda_2, m_l) \right), \quad (18)$$

$$\begin{aligned} C_3^{\text{Po}}(\lambda_1, \lambda_2, \lambda_3; m_l) &= \frac{V}{T} \left(\delta(\lambda_2 - \lambda_1) \delta(\lambda_3 - \lambda_1) \rho(\lambda_1, m_l) \right. \\ &\quad - \frac{V}{TN} \left(\delta(\lambda_2 - \lambda_1) \rho(\lambda_1, m_l) \rho(\lambda_3, m_l) + \delta(\lambda_3 - \lambda_2) \rho(\lambda_1, m_l) \rho(\lambda_2, m_l) \right. \\ &\quad \left. \left. + \delta(\lambda_3 - \lambda_1) \rho(\lambda_1, m_l) \rho(\lambda_2, m_l) \right) \right) \\ &\quad + \left(\frac{V}{TN} \right)^2 2 \rho(\lambda_1, m_l) \rho(\lambda_2, m_l) \rho(\lambda_3, m_l) \Big), \end{aligned} \quad (19)$$

$$\begin{aligned} C_4^{\text{Po}}(\lambda_1, \lambda_2, \lambda_3, \lambda_4; m_l) &= \frac{V}{T} \left(\delta(\lambda_2 - \lambda_1) \delta(\lambda_3 - \lambda_1) \delta(\lambda_4 - \lambda_1) \rho(\lambda_1, m_l) \right. \\ &\quad - \frac{V}{TN} \left(\delta(\lambda_2 - \lambda_1) \delta(\lambda_3 - \lambda_1) \rho(\lambda_1, m_l) \rho(\lambda_4, m_l) + \delta(\lambda_1 - \lambda_4) \delta(\lambda_2 - \lambda_1) \rho(\lambda_1, m_l) \rho(\lambda_3, m_l) \right. \\ &\quad \left. + \delta(\lambda_3 - \lambda_4) \delta(\lambda_2 - \lambda_1) \rho(\lambda_1, m_l) \rho(\lambda_3, m_l) + \delta(\lambda_1 - \lambda_4) \delta(\lambda_3 - \lambda_2) \rho(\lambda_1, m_l) \rho(\lambda_2, m_l) \right. \\ &\quad \left. + \delta(\lambda_2 - \lambda_4) \delta(\lambda_3 - \lambda_2) \rho(\lambda_1, m_l) \rho(\lambda_2, m_l) + \delta(\lambda_3 - \lambda_1) \delta(\lambda_2 - \lambda_4) \rho(\lambda_1, m_l) \rho(\lambda_2, m_l) \right. \\ &\quad \left. \left. + \delta(\lambda_1 - \lambda_4) \delta(\lambda_3 - \lambda_1) \rho(\lambda_1, m_l) \rho(\lambda_2, m_l) \right) \right) \\ &\quad + 2 \left(\frac{V}{TN} \right)^2 \left(\delta(\lambda_2 - \lambda_1) \rho(\lambda_1, m_l) \rho(\lambda_3, m_l) \rho(\lambda_4, m_l) + \delta(\lambda_3 - \lambda_2) \rho(\lambda_1, m_l) \rho(\lambda_2, m_l) \rho(\lambda_4, m_l) \right. \\ &\quad \left. + \delta(\lambda_3 - \lambda_1) \rho(\lambda_1, m_l) \rho(\lambda_2, m_l) \rho(\lambda_4, m_l) + \delta(\lambda_1 - \lambda_4) \rho(\lambda_1, m_l) \rho(\lambda_2, m_l) \rho(\lambda_3, m_l) \right. \\ &\quad \left. + \delta(\lambda_2 - \lambda_4) \rho(\lambda_1, m_l) \rho(\lambda_2, m_l) \rho(\lambda_3, m_l) + \delta(\lambda_3 - \lambda_4) \rho(\lambda_1, m_l) \rho(\lambda_2, m_l) \rho(\lambda_3, m_l) \right) \\ &\quad - 6 \left(\frac{V}{TN} \right)^3 \rho(\lambda_1, m_l) \rho(\lambda_2, m_l) \rho(\lambda_3, m_l) \rho(\lambda_4, m_l) \Big). \end{aligned} \quad (20)$$

As briefly mentioned in the main material N is the number of chiral pairs of Dirac eigenvalues $\{\pm i\lambda_n\}_{n=1}^N$ and it equals to the half number of the lattice sites, $N = N_\sigma^3 N_\tau / 2$. The detailed derivation of C_2^{Po} can be found, e.g. in the appendix of Ref. [32] and C_n^{Po} with $n \geq 3$ can be obtained following the same procedures.

The resulting expressions of χ_{disc} , χ_2 and $\partial^3 \rho(\lambda, m_l) / \partial m_l^3$ in the Poisson limit are listed as follows

$$(\chi_{disc})^{\text{Po}} = 2(\chi_\pi - \chi_\delta) - \frac{V}{TN} \langle \bar{\psi} \psi \rangle^2, \quad (21)$$

$$(\chi_2)^{\text{Po}} = \int_0^\infty d\lambda \frac{16m_l \rho(\lambda, m_l) (\lambda^2 + 3m_l^2)}{(\lambda^2 + m_l^2)^3} - \frac{V}{TN} \langle \bar{\psi} \psi \rangle (6\chi_\pi - 5\chi_\delta) + 2 \left(\frac{V}{TN} \right)^2 \langle \bar{\psi} \psi \rangle^3, \quad (22)$$

$$\begin{aligned} \left(\frac{\partial^3 \rho(\lambda, m_l)}{\partial m_l^3} \right)^{\text{Po}} &= \frac{24m_l \rho(\lambda, m_l)}{(\lambda^2 + m_l^2)^2} \\ &\quad - 12 \frac{V}{TN} \rho(\lambda, m_l) \left(\int_0^\infty d\lambda_1 \frac{2m_l \rho(\lambda_1, m_l)}{(\lambda_1^2 + m_l^2)^2} - \langle \bar{\psi} \psi \rangle \frac{3m_l^2 + \lambda^2}{(\lambda^2 + m_l^2)^2} - \frac{m_l(2\chi_\pi - \chi_\delta)}{\lambda^2 + m_l^2} \right) \\ &\quad + 6 \left(\frac{V}{TN} \right)^2 \rho(\lambda, m_l) \langle \bar{\psi} \psi \rangle \left(\frac{4m_l}{\lambda^2 + m_l^2} \langle \bar{\psi} \psi \rangle + (2\chi_\pi - \chi_\delta) \right) \\ &\quad - 6 \left(\frac{V}{TN} \right)^3 \rho(\lambda, m_l) \langle \bar{\psi} \psi \rangle^3. \end{aligned} \quad (23)$$

$\langle \bar{\psi} \psi \rangle$ vanishes in the chiral limit at $T > T_c$, and this leads to $(\chi_{disc})^{\text{Po}} = 2(\chi_\pi - \chi_\delta)$ as mentioned in the main material.

II. LATTICE QCD CALCULATIONS

II A. Data, Statistics and parameters used in the lattice setup

In this subsection we show the simulation parameters as well as statistics in Table I. We also list the direct measurements of $m_s^2 \chi_{\text{disc}}/T_c^4$ and $m_s^2(\chi_\pi - \chi_\delta)/T_c^4$. In Fig. 4 we show the time history of topological charge obtained from the finest lattices we have, $80^3 \times 16$ lattices with $m_\pi = 80$ MeV and datasets with the smallest quark mass, $56^3 \times 8$ with $m_\pi = 55$ MeV.

β	am_s	am_l	m_π [MeV]	$N_\sigma^3 \times N_\tau$	Chebyshev			Direct	
					p	#conf	#conf	$m_s^2 \chi_{\text{disc}}/T_c^4$	$m_s^2(\chi_\pi - \chi_\delta)/T_c^4$
6.664	0.0514	0.002570	160	$32^3 \times 8$	200000	2000	4054	1.9(1)	2.0(1)
		0.001904	140	$32^3 \times 8$	200000	2000	6707	1.15(8)	1.26(8)
		0.001285	110	$40^3 \times 8$	200000	2000	5625	0.60(3)	0.66(4)
		0.0006425	80	$32^3 \times 8$	300000	1891	3842	0.14(1)	0.18(2)
		0.0006425	80	$40^3 \times 8$	300000	1998	11863	0.20(1)	0.25(2)
		0.0006425	80	$56^3 \times 8$	300000	1992	7341	0.20(1)	0.24(2)
		0.0006425	80	$72^3 \times 8$	300000	2088	5954	0.171(7)	0.20(1)
		0.00032125	55	$56^3 \times 8$	300000	2000	8473	0.059(7)	0.08(1)
7.078	0.034	0.00170	160	$48^3 \times 12$	100000	3614	8507	5.8(5)	5.9(4)
		0.001259	140	$48^3 \times 12$	100000	2000	6575	4.1(2)	4.3(2)
		0.000850	110	$60^3 \times 12$	100000	2990	5314	2.0(2)	2.1(2)
		0.000425	80	$48^3 \times 12$	300000	1993	9021	0.89(8)	1.0(1)
		0.000425	80	$60^3 \times 12$	300000	1998	6746	0.78(6)	0.91(7)
		0.000425	80	$72^3 \times 12$	200000	2365	2365	0.9(1)	1.1(2)
7.356	0.026	0.0013	160	$64^3 \times 16$	100000	2198	3227	12(1)	12(1)
		0.000963	140	$64^3 \times 16$	100000	2370	3639	11(2)	10(2)
		0.000650	110	$64^3 \times 16$	100000	2321	3498	7(1)	7(1)
		0.000325	80	$64^3 \times 16$	500000	2577	4092	3.4(4)	3.7(4)
		0.000325	80	$80^3 \times 16$	300000	3001	5316	3.0(2)	3.7(3)

TABLE I. Summary of lattice parameters, i.e. values of lattice gauge coupling β , strange (am_s) and light quark mass (am_l) in unit of lattice spacing, pion mass (m_π), lattice size ($N_\sigma^3 \times N_\tau$), number of gauge configurations (#conf) used in the direct measurements of chiral observables (Direct) and in the computation of ρ via the Chebyshev polynomial method (Chebyshev) as well as the order of Chebyshev polynomials (p). The direct measurements of $m_s^2 \chi_{\text{disc}}/T_c^4$ and $m_s^2(\chi_\pi - \chi_\delta)/T_c^4$ with $T_c = 132$ MeV are also listed.

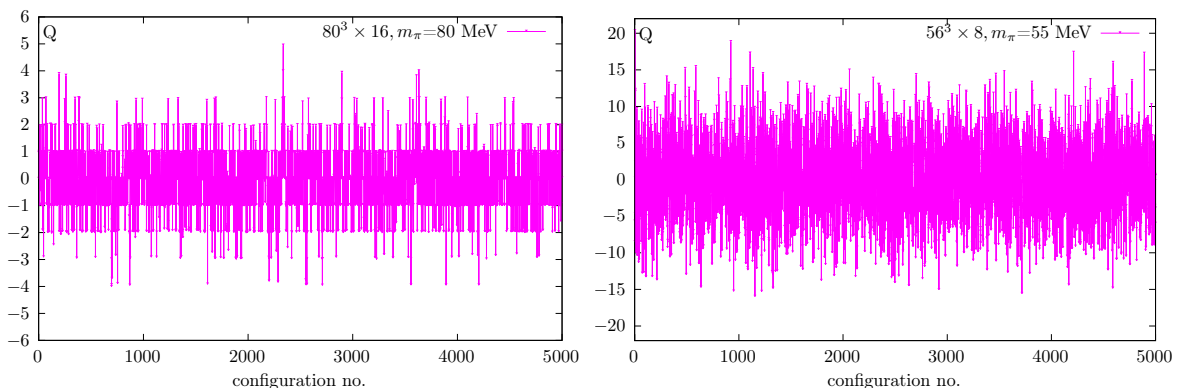


FIG. 4. Left: Time history of topological charge obtained from $80^3 \times 16$ lattices with $m_\pi = 80$ MeV (left) and $56^3 \times 8$ lattices with $m_\pi = 55$ MeV (right) using the Symanzik improved gradient method [59]. Results shown in both plots are obtained at a certain flow time t . The value of t is chosen to be $T\sqrt{8t} = 0.4$ where the topological charge susceptibility already reaches to a plateau in t . This corresponds to $t/a^2 = 0.02N_\tau^2$.

II B. Methodology on the computation of ρ

In this subsection we describe the method we used to compute the spectral density of the lattice Dirac operator as a continuous function over all scales of the complete eigenvalue spectrum. The method has been utilized in the Wilson [41, 55], Domain Wall [42] and staggered [40, 43, 44, 60, 61] discretization schemes. In the following subsection we will also present sanity checks of this method.

Stochastic counting of eigenvalues of a hermitian matrix A in a given interval $[s, t]$ within $[-1, 1]$ can be represented as

$$n[s, t] = \frac{1}{N_r} \sum_{r=1}^{N_r} \xi_r^\dagger h(A) \xi_r, \quad (24)$$

where N_r is the number of random vectors, ξ_r is a Gaussian random noise vector and $h(A)$ is a step function which equals to 1 only in the interval $[s, t]$ and 0 elsewhere. Here $t > s$ is implicitly assumed. In practice, the function $h(A)$ is approximated by the Chebyshev polynomial

$$h(A) = \sum_{j=0}^p g_j^p \gamma_j T_j(A). \quad (25)$$

The coefficients g_j^p and γ_j are known numbers once the interval $[s, t]$ is given, and p is the order of Chebyshev polynomials. As the expansion of $h(A)$ has harmful oscillations near the boundaries g_j^p is introduced [62] here to suppress this behavior. $T_j(A)$ is the Chebyshev polynomial of operator A and it can be constructed by the following recursion relation

$$T_0(A) = 1, \quad T_1(A) = A, \quad T_j(A) = 2AT_{j-1}(A) - T_{j-2}(A) \quad (j \geq 2). \quad (26)$$

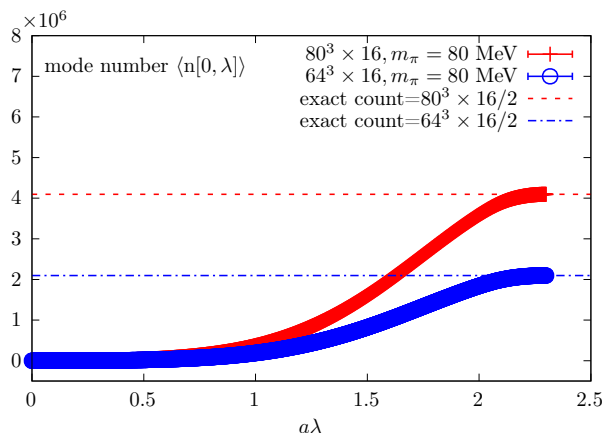


FIG. 5. Averaged mode number $n[0, \lambda]$ over configurations as a function of λ in unit of lattice spacing a computed on $80^3 \times 16$ and $64^3 \times 16$ lattices with $m_\pi = 80$ MeV. The mode numbers obtained from $80^3 \times 16$ and $64^3 \times 16$ lattices reach to the numbers of $80^3 \times 16/2$ and $64^3 \times 16/2$, respectively, in the large λ limit for positive λ as expected.

The above deviation is based on the assumption that all the eigenvalues of A are restricted in the range of $[-1, 1]$. In order to apply the eigenvalue filtering method to calculate the Dirac spectrum, we therefore define

$$A = \frac{\mathcal{D}_{stag}^\dagger \mathcal{D}_{stag} - \frac{(\tilde{\lambda}_{\max} + \tilde{\lambda}_{\min})}{2} \mathbb{1}}{\frac{(\tilde{\lambda}_{\max} - \tilde{\lambda}_{\min})}{2} \mathbb{1}}, \quad (27)$$

such that the eigenvalues of A are all distributed in $[-1, 1]$. Here \mathcal{D}_{stag} stands for the massless Dirac matrix in the staggered discretization scheme, i.e. \mathcal{D}_{stag} is defined as M_{stag} in the case of vanishing quark mass. Substituting the expression of $h(A)$ (Eq. 25) into the stochastic estimator (Eq. 24) we can obtain the mode number $n[s, t]$ for a given gauge configuration,

$$n[s, t] = \frac{1}{N_r} \sum_{r=1}^{N_r} \sum_{j=0}^p g_j^p \gamma_j \xi_r^\dagger T_j(A) \xi_r. \quad (28)$$

Once we get the mode number $n[s, t]$, $\rho_U(\lambda) = \sum_j \delta(\lambda - \lambda_j)$ can be easily constructed as

$$\rho_U(\lambda) = \frac{1}{4} \frac{n[s, t]}{2\delta\lambda}, \quad (29)$$

where the factor $1/4$ accounts for the fourth-root arising from the staggered discretization scheme, the factor 2 in the denominator is due to the positive and negative eigenvalue pairs, $\delta\lambda$ is the bin-size, and $\lambda \equiv \lambda^{|\mathcal{D}_{stag}|}$ is related to $\tilde{\lambda}$ being the eigenvalues of matrix $\mathcal{D}_{stag}^\dagger \mathcal{D}_{stag}$ as follows

$$\begin{aligned} \lambda &= \sqrt{\tilde{\lambda}} = \left[s \left(\tilde{\lambda}_{\max} - \tilde{\lambda}_{\min} \right) / 2 + \left(\tilde{\lambda}_{\max} + \tilde{\lambda}_{\min} \right) / 2 \right]^{1/2}, \\ \lambda + \delta\lambda &= \sqrt{\tilde{\lambda} + \delta\tilde{\lambda}} = \left[t \left(\tilde{\lambda}_{\max} - \tilde{\lambda}_{\min} \right) / 2 + \left(\tilde{\lambda}_{\max} + \tilde{\lambda}_{\min} \right) / 2 \right]^{1/2}. \end{aligned} \quad (30)$$

In our work $\tilde{\lambda}_{\min}$ being the minimum value of $\tilde{\lambda}$ is set to 0 and $\tilde{\lambda}_{\max}$ being the maximum value of $\tilde{\lambda}$ is estimated by the power method [63]. The ensemble averaged $n[0, \lambda]$ obtained from two different volumes of lattices is demonstrated in Fig. 5.

Once ρ_U is obtained it is straightforward to compute the Dirac eigenvalue spectrum ρ as T/V multiplied by the average of ρ_U over gauge configurations, i.e. $\rho \equiv \frac{T}{V} \langle \rho_U \rangle$ (cf. Eq. 1). Similarly one can also compute the correlation functions as $C_n(\lambda_1, \dots, \lambda_n; m_l) = \langle \prod_{i=1}^n [\rho_U(\lambda_i) - \langle \rho_U(\lambda_i) \rangle] \rangle$. The error analyses of ρ and C_n presented in our paper are all done using the Jackknife method.

For demonstration we show ρ and $C_2(\lambda_1, \lambda_2)$ obtained from $80^3 \times 16$ lattices with $m_\pi = 80$ MeV in the left and right panel of Fig. 6, respectively.

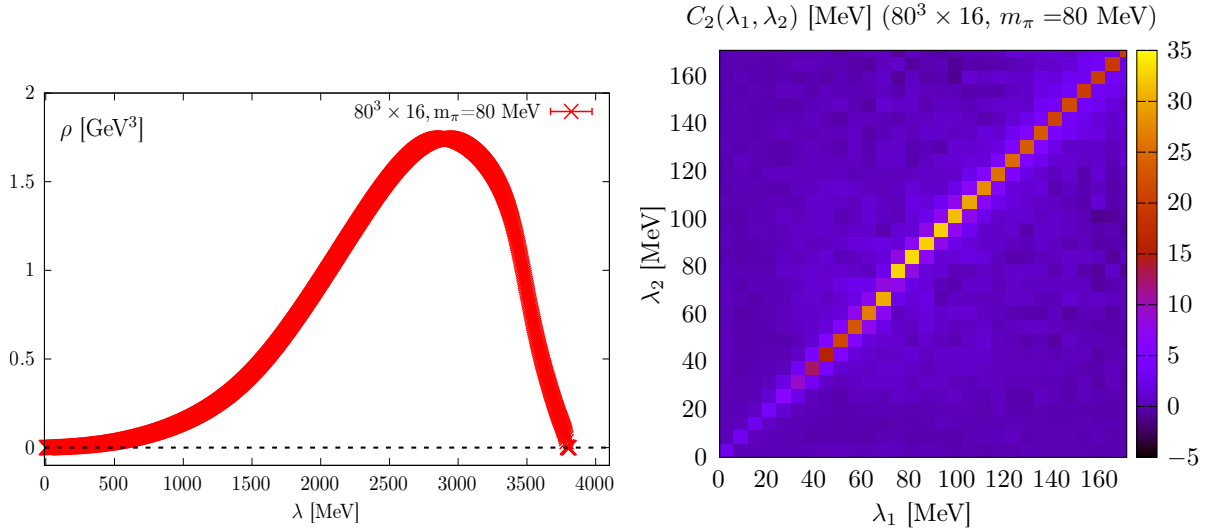


FIG. 6. Dirac eigenvalue spectrum ρ (left) and the two-point correlation function C_2 (right) obtained on $80^3 \times 16$ lattices with $m_\pi = 80$ MeV.

II C. Sanity checks of $\partial^n \rho / \partial m_l^n$

As from the definition of C_n the following constraint is fulfilled

$$\int_0^\infty d\lambda_i C_n(\lambda_1, \lambda_2, \dots, \lambda_i, \dots, \lambda_n; m_l) = 0, \quad (31)$$

where λ_i stands for any one of λ 's. Consequently

$$\int_0^\infty d\lambda \partial^n \rho(\lambda, m_l) / \partial m_l^n = 0, \quad \text{with } n \geq 1 \text{ and } n \in \mathbb{Z}. \quad (32)$$

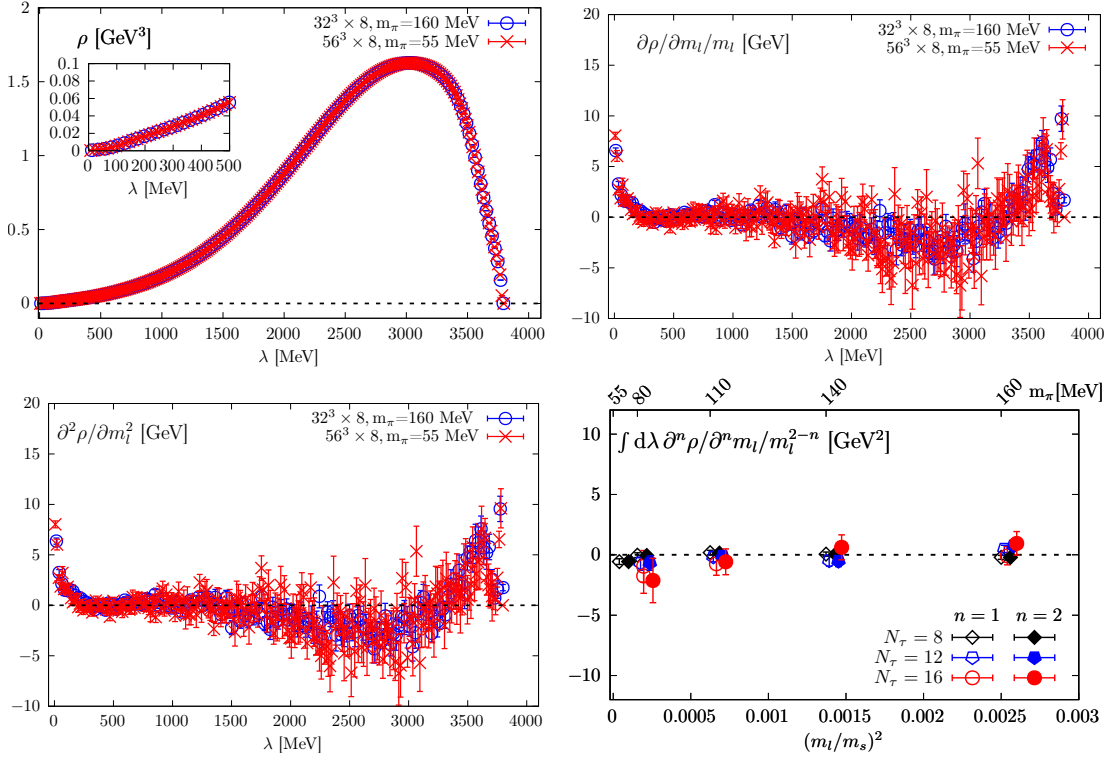


FIG. 7. ρ (top left), $m_l^{-1} \partial \rho(\lambda, m_l) / \partial m_l$ (top right) and $\partial^2 \rho(\lambda, m_l) / \partial m_l^2$ (bottom left) as a function of λ in a complete region of λ . The insert in the top left panel shows a blow-up of ρ in the region of $\lambda \in [0, 500]$ MeV. In these three plots results are all obtained from $N_\tau = 8$ lattices with $m_\pi = 160$ and 55 MeV. The bottom right panel shows the integration of $\int d\lambda m_l^{n-2} \partial^n \rho(\lambda, m_l) / \partial m_l^n$ for $n = 1$ and 2 obtained at all the quark masses and lattice spacings with the largest N_σ available. The filled symbols are slightly shifted horizontally for visibility.

Eq. 32 thus suggests that $\partial^n \rho(\lambda, m_l) / \partial m_l^n$ with $n \geq 1$ must either contain both negative and positive parts in λ or vanish for all values of λ .

Here we demonstrate the complete spectrum of ρ and its first and second derivatives in m_l obtained from $N_\tau = 8$ lattices with $m_\pi = 160$ and 55 MeV. We first show the complete spectrum of ρ in the top left panel of Fig. 7. It can be found that the m_l dependence can be hardly observed from ρ directly. In the top right and bottom left panels of Fig. 7 we show complete spectrum of $m_l^{-1} \partial \rho(\lambda, m_l) / \partial m_l$ and $\partial^2 \rho(\lambda, m_l) / \partial m_l^2$, respectively. It can be clearly seen that both $m_l^{-1} \partial \rho(\lambda, m_l) / \partial m_l$ and $\partial^2 \rho(\lambda, m_l) / \partial m_l^2$ possess negative and positive values in the complete λ region. In the bottom right panel of Fig. 7 we show the integrations $\int d\lambda m_l^{n-2} \partial^n \rho(\lambda, m_l) / \partial m_l^n$ for $n = 1$ and 2 obtained at all the quark masses and lattice spacings with the largest N_σ available. It can be observed that all these integrations are consistent with zero within errors as expected (cf. Eq. 32).

The final results of ρ depend on the order of Chebyshev polynomials p . We show in Fig. 8 the p -dependence of $\chi_\pi - \chi_\delta$ and χ_{disc} computed via Eq. 9 and Eq. 10, respectively, from $64^3 \times 16$ lattices with $m_\pi = 80$ MeV. It can be seen that with $p \geq 100000$ results of both $\chi_\pi - \chi_\delta$ and χ_{disc} start to saturate and agree within errors with the results obtained from direct measurements.

III. RESULTS

III A. Supplemental materials to Fig. 1

We show similar results to the left panel of Fig. 1 but for $N_t = 12$ and 16 in the left and right panels of Fig. 9, respectively. The general feature observed in the left panel of Fig. 1 persists in the results obtained from finer lattices.

Supplementary to the results shown in the middle panel of Fig. 1 we show results of $\frac{\partial^2 \rho}{\partial m_l^2}$ and $\frac{\partial^3 \rho}{\partial m_l^3}$ (inset) at $m_\pi = 110$

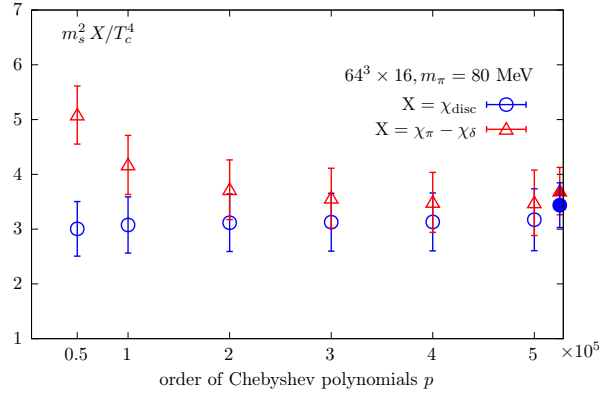


FIG. 8. Dependence of χ_{disc} and $\chi_{\pi} - \chi_{\delta}$ obtained from ρ and $\partial\rho/\partial m_l$ on the order of Chebyshev polynomials p . The corresponding filled symbols located on the most right hand side denote the results obtained from direct measurements. The computation were performed on $64^3 \times 16$ lattices with $m_{\pi} = 80$ MeV.

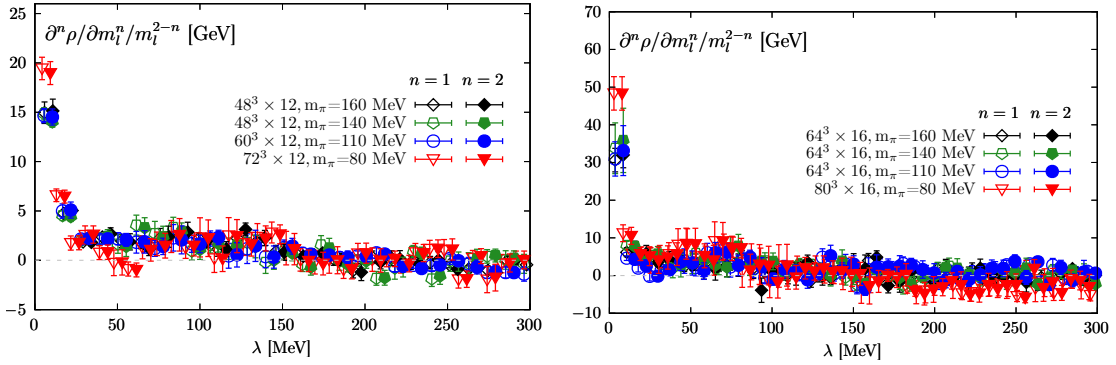


FIG. 9. Light sea quark mass dependence of $m_l^{-1} \partial\rho(\lambda, m_l)/\partial m_l$ (open symbols) and $\partial^2\rho(\lambda, m_l)/\partial m_l^2$ (filled symbols) using $N_{\tau} = 12$ (left) and $N_{\tau} = 16$ (right) lattices. In all cases, results are obtained at $T \approx 205$ MeV and the filled symbols have been slightly shifted horizontally for visibility.

MeV (left), 140 MeV (middle) and 160 MeV (right) in Fig. 10.

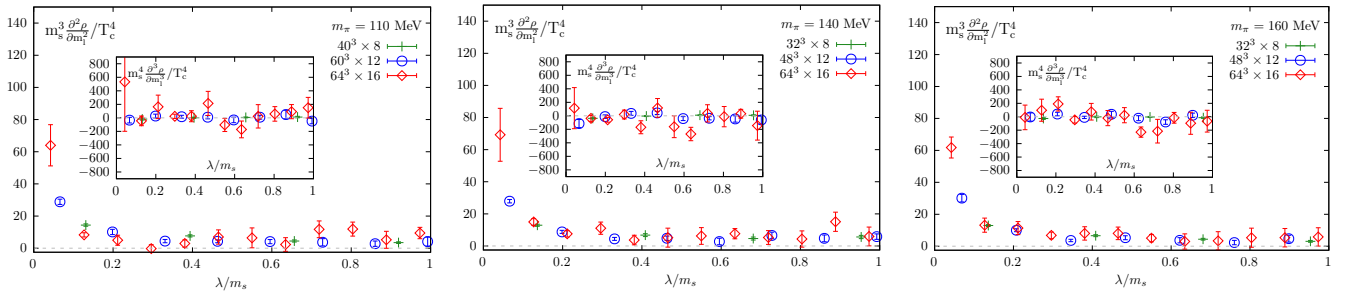


FIG. 10. Lattice spacing dependence of $\partial^2\rho(\lambda, m_l)/\partial m_l^2$ and $\partial^3\rho(\lambda, m_l)/\partial m_l^3$ (inset) for $m_{\pi} = 110$ MeV (left), 140 MeV (middle) and 160 MeV (right). In all cases, results are obtained at $T \approx 205$ MeV.

We show in Fig. 11 the lattice spacing dependence of $m_l^{-1} \partial\rho(\lambda, m_l)/\partial m_l$ and $\partial^2\rho(\lambda, m_l)/\partial m_l^2$ for $m_{\pi} = 80$ MeV at the same bin-size in λ/m_s as used on $N_{\tau} = 16$ lattices in the main text. It can be seen that the feature of a sharper peak persists towards the continuum limit. It is expected that using this same bin-size in λ/m_s the directly measured chiral observables for $N_{\tau} = 12$ and $N_{\tau} = 8$ lattices cannot be reproduced.

Supplementary to the results shown in the right panel of Fig. 1 we show similar results but for $m_{\pi}=110$ MeV (left), 140 MeV (middle) and 160 MeV (right) in Fig. 12.

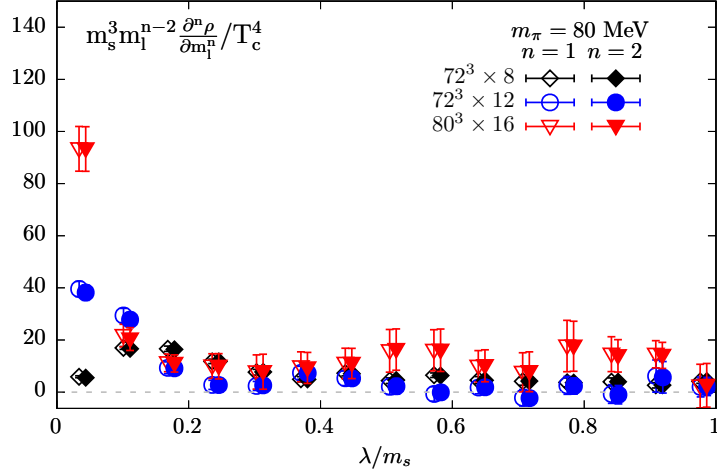


FIG. 11. Lattice spacing dependence of $m_l^{-1} \partial \rho(\lambda, m_l) / \partial m_l$ (open symbols) and $\partial^2 \rho(\lambda, m_l) / \partial m_l^2$ (filled symbols) for $m_\pi = 80$ MeV at the same bin-size in λ/m_s as used on $N_\tau = 16$ lattices in the main text. The filled symbols have been slightly shifted horizontally for visibility.

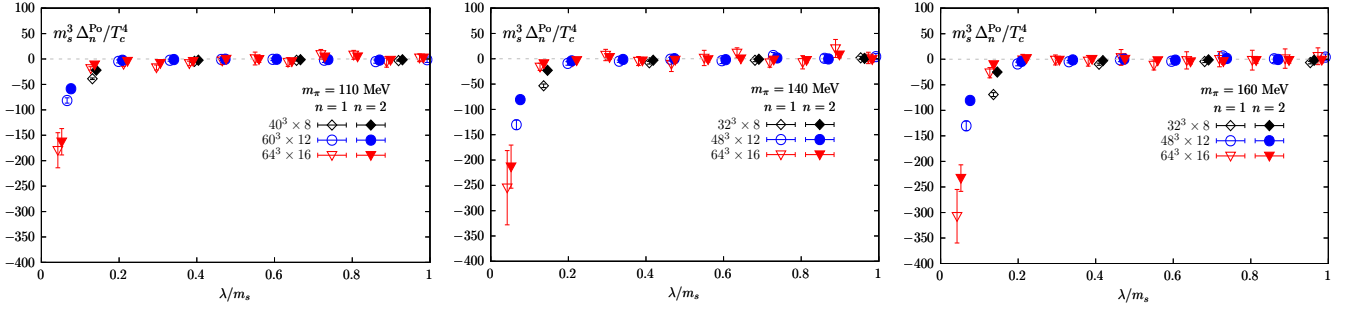


FIG. 12. The differences $\Delta_n^{Po} = m_l^{n-2} [\partial^n \rho / \partial m_l^n - (\partial^n \rho / \partial m_l^n)^{Po}]$ (cf. Eq. 11 and Eq. 12), for $m_\pi = 110$ MeV (left), 140 MeV (middle) and 160 MeV (right).

III B. Supplemental materials to Fig. 2

III B1. Volume dependence of the two $U(1)_A$ measures

We show the volume dependence of $\chi_\pi - \chi_\delta$ and χ_{disc} at $m_\pi = 80$ MeV in the left and right panels of Fig. 13, respectively. One can observe that the volume dependences of these two quantities are mild.

III B2. Reproduction of $\langle \bar{\psi} \psi \rangle$ and χ_2 via ρ and $\frac{\partial^2 \rho}{\partial m_l^2}$

We show the quark mass dependence of light quark chiral condensate in the left panel of Fig. 14. The bin-size of ρ , as mentioned in the main text, was fixed by reproducing the value of $\chi_\pi - \chi_\delta$ through our paper. One can see that the chiral condensate computed from the stochastic estimates of $\text{Tr} M^{-1}$ (cf. Eq. 14) can be well reproduced by $\rho(\lambda, m_l)$ via Eq. 13. The linear fits denoted by the dashed lines give a good description of the data. As seen from the fit results light quark chiral condensates at each lattice spacing vanish in the chiral limit. This is expected in the chiral symmetric phase. Although the data points and fits shown in the left plot are obtained only from the largest N_σ available, the volume dependence of chiral condensate is mild as shown in the right panel of Fig. 14.

By using the same bin-size as that used for the reproduction of $\chi_\pi - \chi_\delta$ in the numerical integration we observe from Fig. 15 that the direct measurement of χ_2 (cf. Eq. 16) can be well reproduced by $\partial^2 \rho / \partial m_l^2$ via Eq. 15. It can also be seen that this quantity has mild volume dependence at $m_\pi = 80$ MeV.

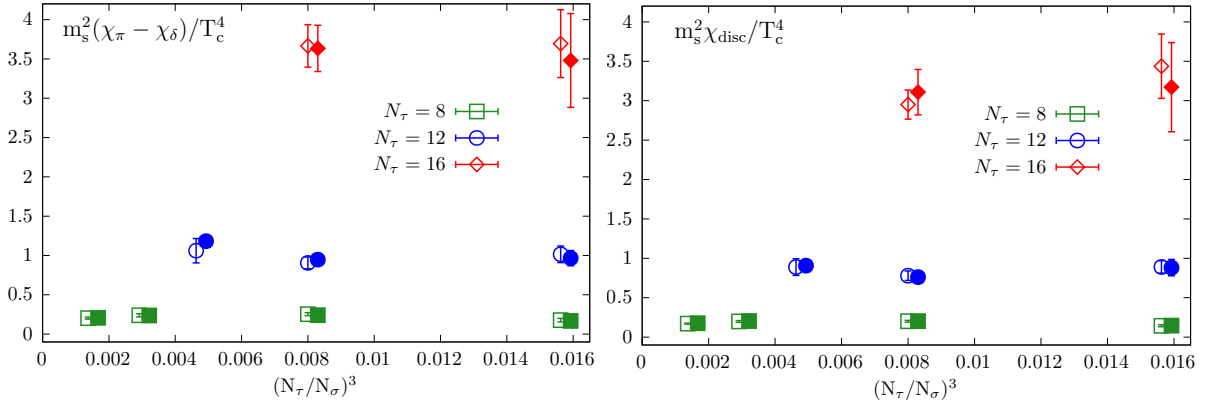


FIG. 13. Volume dependences of $\chi_\pi - \chi_\delta$ (left) and χ_{disc} (right) obtained at each lattice spacing and $m_\pi = 80$ MeV. The factor of m_s^2/T_c^4 is used to make the quantities renormalization group invariant and dimensionless. In both plots the open symbols denote direct measurements while the filled symbols slightly shifted horizontally for visibility denote the corresponding results obtained from ρ and $\partial\rho/\partial m_l$.

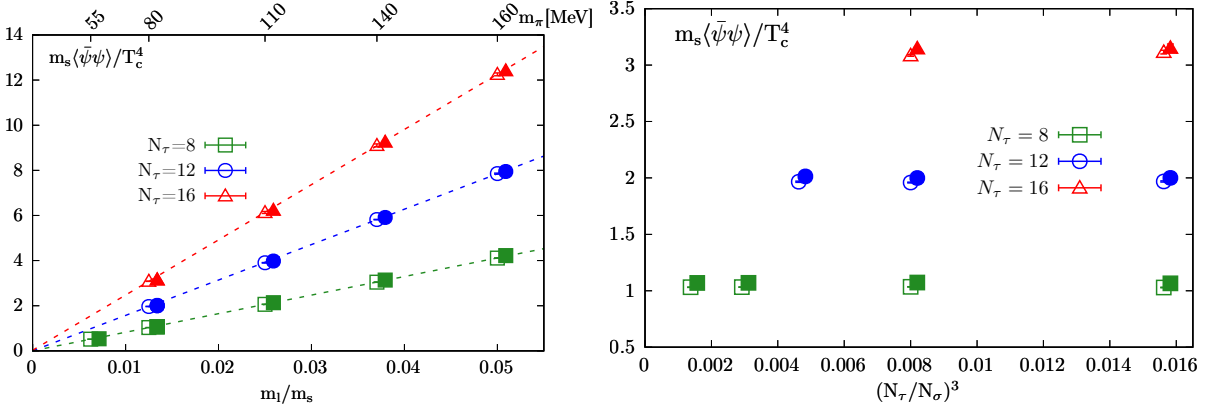


FIG. 14. Left: $m_s\langle\bar{\psi}\psi\rangle/T_c^4$ as a function of light quark mass at different lattice spacings at $m_\pi = 80$ MeV obtained from the largest volume available. The dashed lines denote linear fits in quark mass to the directly measured $\langle\bar{\psi}\psi\rangle$. Right: Volume dependence of $m_s\langle\bar{\psi}\psi\rangle/T_c^4$ at different lattice spacings with $m_\pi = 80$ MeV. In both plots the open symbols denote results obtained from stochastic estimates of the trace of the inverse fermion matrix M^{-1} (cf. Eq. 14) while the corresponding filled symbols slightly shifted horizontally for visibility denote results obtained from ρ via Eq. 13.

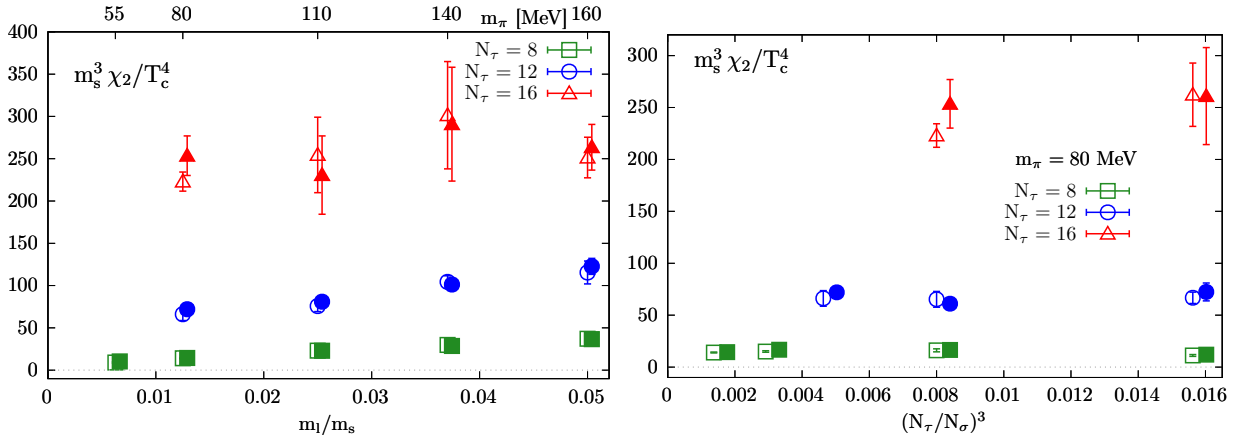


FIG. 15. Left: Lattice spacing and quark mass dependences of $m_s^3\chi_2/T_c^4$ obtained from the largest N_σ available. Right: Volume dependence of $m_s^3\chi_2/T_c^4$ at $m_\pi = 80$ MeV. In both plots the open symbols denote direct measurements from M^{-1} (cf. Eq. 16) while the corresponding filled symbols slightly shifted horizontally for visibility denote the corresponding results obtained from $\partial^2\rho/\partial m_l^2$ via Eq. 15.

III B3. Infrared contributions to the two $U(1)_A$ measures

To check the infrared contribution to the two $U(1)_A$ measures we also introduce an upper cutoff in λ , i.e. λ_{cut} in the integrations of following expressions,

$$\begin{aligned} (\chi_\pi - \chi_\delta)(\lambda_{cut}) &= \int_0^{\lambda_{cut}} d\lambda \frac{8m_l^2 \rho}{(\lambda^2 + m_l^2)^2}, \\ \chi_{disc}(\lambda_{cut}) &= \int_0^{\lambda_{cut}} d\lambda \frac{4m_l}{\lambda^2 + m_l^2}. \end{aligned} \quad (33)$$

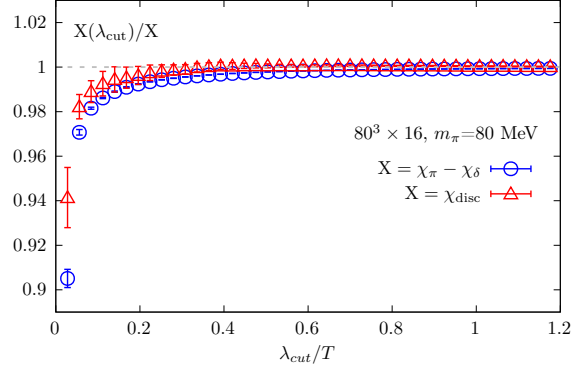


FIG. 16. Ratios of $\chi_\pi - \chi_\delta$ and χ_{disc} obtained from ρ and $\partial\rho/\partial m_l$ with different values of upper limit of the integration λ_{cut} to their corresponding values obtained using a complete region of λ in the integration.

We show the λ_{cut} dependences of the ratios $(\chi_\pi - \chi_\delta)(\lambda_{cut})$ and $\chi_{disc}(\lambda_{cut})$ to their corresponding values obtained using the complete λ region in the integration in Fig. 16. It can be found that the infrared part, i.e. $\lambda/T \lesssim 1$ of Dirac eigenvalue spectrum gives the dominate contributions to both $\chi_\pi - \chi_\delta$ and χ_{disc} .

III C. Supplemental materials to Fig. 3

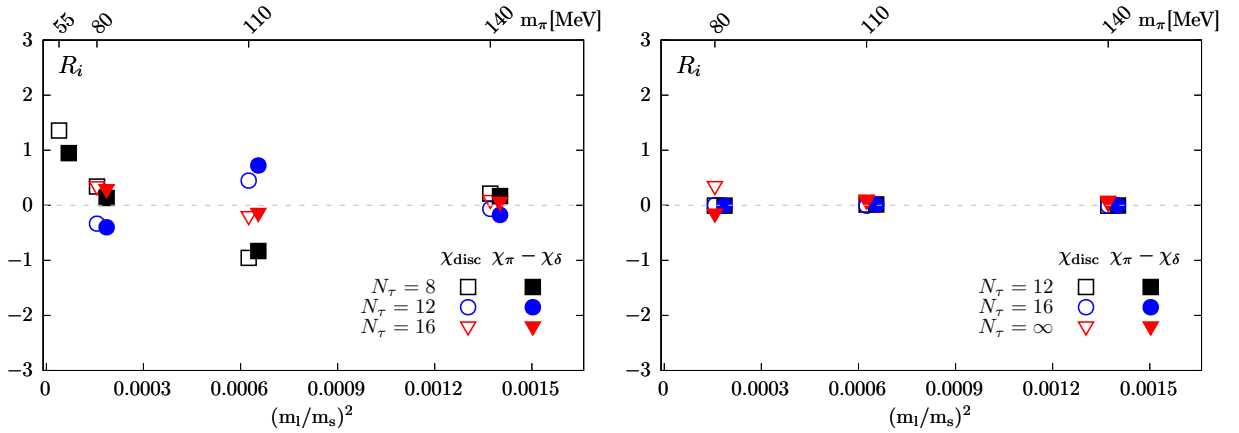


FIG. 17. R_i obtained from the joint fit (left) and from the sequential fit (right) with firstly continuum extrapolations and then chiral extrapolations for both χ_{disc} and $\chi_\pi - \chi_\delta$ performed in Fig. 3 in the main material.

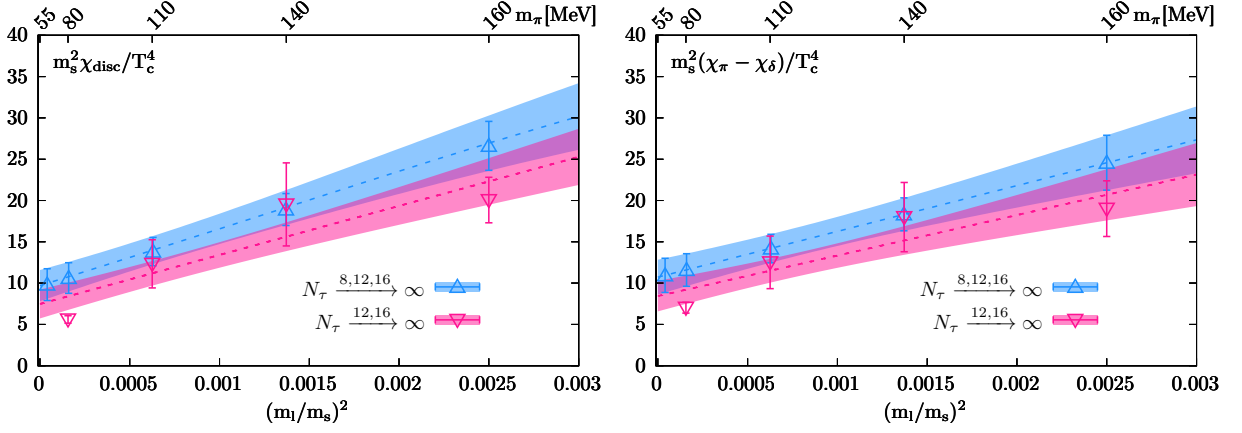


FIG. 18. Same as Fig. 3 in the main material but with data at $m_\pi = 160$ MeV included in the extrapolations.

To check the quality of extrapolations we investigate on the following quantity

$$R_i = \frac{Y_i - Y_{i,fit}}{\sqrt{\sigma_{Y_i}^2 + \sigma_{Y_{i,fit}}^2}}. \quad (34)$$

Here Y_i and σ_{Y_i} stand for mean values and Jackknife errors of the data points obtained at each lattice spacing and quark mass, respectively, while $Y_{i,fit}$ and $\sigma_{Y_{i,fit}}$ are corresponding mean values and errors obtained from the fit to data. The integer subscript i runs from 1 to the number of data points used in the fit.

In Fig. 17 we show R_i obtained from the extrapolations performed in Fig. 3 in the main material. I.e. we show R_i obtained from joint fits (left), and from the sequential fit (right) with firstly continuum extrapolations and then chiral extrapolations for both χ_{disc} and $\chi_\pi - \chi_\delta$. It can be seen that values of R_i scatter around 0.

We perform the same extrapolations as being done in Fig. 3 in the main material but with data at $m_\pi = 160$ MeV included. Results for χ_{disc} and $\chi_\pi - \chi_\delta$ are shown in the left and right panels of Fig. 18, respectively. It can be seen that the two $U(1)_A$ measures remain degenerate within errors in the continuum and chiral limit. It can also be observed that both mean values become larger by about 35-73% while errors remain similar as compared to the case without $m_\pi = 160$ MeV data included in the extrapolations. Thus χ_{disc} and $\chi_\pi - \chi_\delta$ deviate further away from zero at a (4-5)- σ level. This is expected as that $m_\pi = 160$ MeV data at each lattice spacing grows slower than linearly in quark mass squared (*cf.* Fig. 2 in the main material) and including it in the extrapolation could bring the values of χ_{disc} and $\chi_\pi - \chi_\delta$ larger in the chiral limit. To better describe the data at $m_\pi = 160$ MeV a fit ansatz including higher order corrections in quark mass squared is needed.